Journal of Materials Chemistry C

Accepted Manuscript

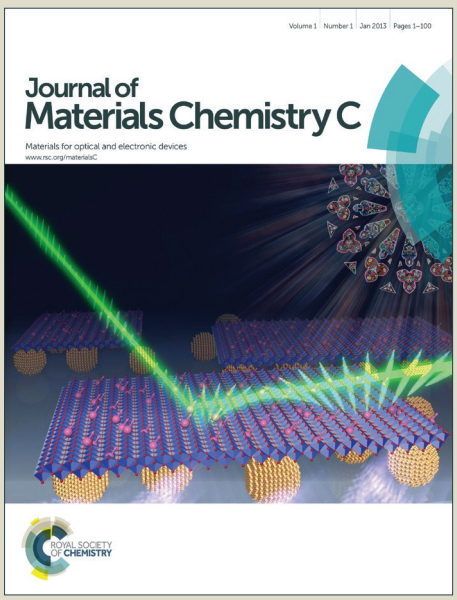

This is an *Accepted Manuscript*, which has been through the Royal Society of Chemistry peer review process and has been accepted for publication.

Accepted Manuscripts are published online shortly after acceptance, before technical editing, formatting and proof reading. Using this free service, authors can make their results available to the community, in citable form, before we publish the edited article. We will replace this *Accepted Manuscript* with the edited and formatted *Advance Article* as soon as it is available.

You can find more information about *Accepted Manuscripts* in the Information for Authors.

Please note that technical editing may introduce minor changes to the text and/or graphics, which may alter content. The journal's standard Terms & Conditions and the Ethical guidelines still apply. In no event shall the Royal Society of Chemistry be held responsible for any errors or omissions in this *Accepted Manuscript* or any consequences arising from the use of any information it contains.

ROYAL SOCIETY OF CHEMISTRY

www.rsc.org/materialsC

Table of contents entry for the manuscript:

"Suppression of nanowires clustering in hybrid energy harvesters"

The performance of hybrid energy harvesters based on ZnO nanowire arrays has been effectively enhanced by the introduction of PMMA.

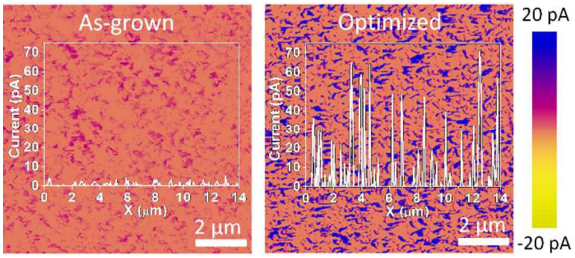

Journal of Materials Chemistry C Accepted Manuscript

Suppression of nanowires clustering in hybrid energy harvesters

*Chengbin Pan[1], Jianchen Hu[1], Enric Grustan-Gutierrez[1], Minh Tuan Hoang[2], Huiling Duan[3], Julien Yvonnet[2], Alexander Mitrushchenkov[2], Gilberte Chambaud[2], Mario Lanza[1,]**

[1]Institute of Functional Nano & Soft Materials (FUNSOM), Collaborative Innovation Center of the Ministry of Education, Soochow University, 199 Ren-Ai Road, Suzhou, 215123,China. [2]Université Paris-Est, Laboratoire Modélisation et Simulation Multi Echelle, MSME UMR 8208 CNRS, 5 bd Descartes, F-77454 Marne-la-Vallée, France. [3]State Key Laboratory for Turbulence and Complex System, Department of Mechanicsand Engineering Science, CAPT, College of Engineering, Peking University, Beijing 100871, China.

* Corresponding Author Email: mlanza@suda.edu.cn

KEYWORDS: Nanowire arrays; Clustering suppression; Finite Element Method calculations; Piezoelectricity; Photo-electricity

ABSTRACT: In energy harvesters using arrays of nanowires (NWs), a larger density of NWs should imply higher performance, but in reality the efficiency of the cells is always deteriorated due to NWs collision. Impeding the formation of NW clusters in highly populated arrays is essential to ensure effective NWs movement and provide high surface area. Here we present a cost-effective methodology to avoid NWs clustering in highly populated arrays of nanowires. First, a flexible polymer is intercalated between the NWs by spin coating, and then its height is

Journal of Materials Chemistry C Accepted Manuscript

tuned with a controlled oxygen plasma etching step. The resulting optimized energy harvesters show an enhancement of a factor 80 in the piezoelectric effect, as well as notable improvement in the photoelectric response. The relationship between the height of the intercalated polymer and the piezo potential produced by the nanowires is simulated by the finite element method calculations, which support the experimental observations.

1. Introduction

The use of nanowires (NWs) in the design of advanced energy harvesters has gained massive interest during the last years due to their easy fabrication and versatility [1-7]. One of the most explored configurations is the zinc oxide NWs array, which has allowed the fabrication of many types of hybrid nanogenerators [8-10] and detectors [11-13]. When sufficient mechanical energy is applied to a ZnO nanowire anchored to a substrate, the freestanding end can bend, generating a voltage difference between the compressed and elongated surfaces by piezoelectric effect [14]. At the same time, if the ZnO nanowire is illuminated, additional photoelectric potential can be induced on its surface [15-18]. Up to now, a variety of methods have been developed to synthesize piezoelectric NW arrays, including chemical hydrothermal synthesis [19], microwave–assisted hydrothermal synthesis [20], thermal evaporation synthesis [13], vapor-confined face-to-face annealing technique [21], pulsed direct current magnetron sputtering [22], radio-frequency magnetron sputtering technique [23], electron-beam template lithography [24] and chemical vapor deposition [25]. However, thermal evaporation synthesis, vapor-confined face-to-face annealing and chemical vapor deposition normally require high operation temperatures and long production times (due to heating and cooling) resulting in high energy consumption and low productivity. Microwave-

Journal of Materials Chemistry C Accepted Manuscript

assisted hydrothermal method, seed-layer-assisted electrochemical deposition, pulsed direct current magnetron sputtering and radio-frequency magnetron sputtering may remarkably decrease the synthesis temperature, but the demand for external electric field makes the fabrication procedure even more complex; furthermore, the cost of electron-beam template lithography is too high to be used for large scale experiments. Chemical hydrothermal synthesis is a good solution due to its low cost and operation temperature. Nevertheless, some problems limiting the performance of these devices still remain unsolved, including a poor NW-electrode interface (which limits charge transfer [26-29]) and NW-to-NW collision (which restricts the movement of the nanowires, as well as reduces the amount of surface area available for photoelectric effect). Both factors make the large current densities generated at the nanoscale (which have been estimated to be around 5 A/cm^2) cannot be driven out, resulting in much lower output currents of just a few $\mu A/cm^2$. While intensive efforts have been dedicated on enhancing the nanowires-electrode interface (including the use of paired nanotip-to-NW brushes [26-27] and flexible graphene electrodes [28-29]) much less progress has been reported on avoiding NW-to-NW collision. One option is to reduce the density of nanowires [19], but that also reduces the amount of energy generated in the nanogenerator. Therefore, developing a strategy for avoiding NWs collision in dense arrays of nanowires is highly desirable.

In this work, a simple and cost-effective methodology to avoid nanowire clustering is developed by inserting a layer of polymethylmethacrylate (PMMA) between the NWs using spin coating technique and partially etching it with oxygen plasma to tune its height. PMMA spin coating was previously used by Gao et al. [30] in low density arrays of nanowires to reinforce the NW/substrate bonding, which provided higher mechanical stability. In our case, the goal of the PMMA coating

Journal of Materials Chemistry C Accepted Manuscript

is to separate the nanowires and avoid clustering in high density NW arrays, and we further optimize the performance of the cell by tuning the height of the PMMA layer with a controlled oxygen plasma etching step. The optimized nanogenerators overcome the performance of their standard counterparts in a factor of 80, which is provided by the effective separation between the nanowires, enhancing both piezo and photoelectric effects. We corroborate the experimental observations using finite element method simulations, and conclude that the optimization of the spin coating and etching parameters are key elements to achieve high performance. This easy, rapid and cheap method not only has no request for high operation temperature (in fact, it even does not need annealing), but it also avoids the use of high external electrical fields, which greatly reduce the fabrication costs.

2. Experimental Section

2.1. Synthesis of ZnO nanowire arrays

Silicon wafers were cleaned by a standard process: each wafer was individually ultrasonicated in acetone, ethanol and deionized water (10 minutes for each step), and dried with a nitrogen gun. A 5 nm thick Zinc Oxide (ZnO) seed layer was deposited on the surface of the silicon substrate by magnetron plasma sputtering (Kurt J. Lesker, PVD75). In the next step, the nutrient solution was prepared, by diluting 0.01 mol $Zn(NO_3)_2 \cdot 6H_2O$, 0.01 mol hexamethylenetetramine (HMTA) and 10 mL ammonium hydroxide in 100 mL deionized water. Finally, the bottom of the Si substrate was fixed onto a standard glass slide and immersed in the nutrient solution. The growth of ZnO nanowires was carried out in a sealed teflon-lined stainless steel autoclave

Journal of Materials Chemistry C Accepted Manuscript

(Shanghai Jing Hong laboratory instrument corporation, KH100) at 95 ºC for 3 hours. The as-grown ZnO NWs were cleaned by deionized water and dried with a nitrogen gun.

2.2. Novel steps to avoid nanowire clustering

The yielded NWs arrays were spin-coated with PMMA using different speeds and times (2500 rpm during 1 minute, 2500 rpm during 3minutes and 4000 rpm during 3 minutes, respectively). The spinner used was from Siyouyen (KW-4A). The PMMA used was composed with 1 g PMMA powder and 25 ml methyl-phenoxide. The dense PMMA gel allocates in between the nanowires, leading to their effective separation, which was corroborated using a Scanning Electron Microscope (SEM) coupled with Electron Dispersive X-Ray Spectroscopy (EDS) from Quanta 200FEG. The relationship between the PMMA thickness and the piezotronic effect generated by the NWs is explored using a series of time-dependent oxygen plasma etching experiments. The samples permeated with PMMA were etched by oxygen plasma treatment at a power of 400 W for 0.5, 1, 1.5, 2, 3 and 4 minutes respectively. The schematic of the fabrication process is shown in Figure 1a.

2.3. Morphological and electronic characterization

The morphology and electronic properties of the nanogenerators have been investigated with a field-emission SEM from Zeiss (model Supra 55), a Quanta 200FEG Scanning Electron Microscope, and a conductive atomic force microscopy (CAFM) from Bruker (model MultiMode V). The Pt-Ir coated silicon tips used for CAFM measurement were also from Bruker

Journal of Materials Chemistry C Accepted Manuscript

(model SCM-PIC), with a spring constant of 0.2 N/m. The light bank connected to the CAFM for photoelectric measurements is a Dolan-Jenner (model MI-152) which supplies a light intensity of 1170 μW at 100%. Additional chemical information about the samples was gained using the Electron Dispersive X-Ray Spectroscopy (EDX) tool integrated in the Quanta 200FEG SEM, using an accelerating voltage of 20 kV, spot size of 3 nm, temperature of 20 ºC, chamber pressure of 5.4×10^{-5} Pa, work distance of 10 mm. X-ray detector limit of 0.1 %, resolution of 129 eV. The EDX detector was used imposing an angle of 30° with the horizontal, and the equipment was calibrated by two standard samples before the measurement. Additional structural characterization of the NWs was conducted with a Tecnai G2 F20 High-resolution Transmission Electron Microscope (HRTEM) using standard copper grid and a field voltage of 160 KV. Two programs were used to analyze the data collected with the CAFM: the NanoScope Analysis 1.4 (Build R2.82860) and the Nanotec WSxM 5.0 (develop 7.0).

2.4. Finite element method calculations

A classical finite element method was used to solve the equations describing the piezoelectric nanowires array model. Equations describing quasi-static piezoelectricity in solids are given, assuming zero volumetric distribution of charges and neglecting body forces, by the Maxwell equation and balance of momentum:

$$D_{i,i} = 0 \; in \Omega, \quad \sigma_{ij,j} = 0 \; in \; \Omega,$$

Journal of Materials Chemistry C Accepted Manuscript

where D and σ denote electric displacement and Cauchy stress, respectively, and where Ω defines the spatial domain containing the different constituents of the system (nanowires and polymer). The constitutive relationships are provided by:

$$\sigma_{ij} = C_{ijkl}\varepsilon_{ij} - e_{ijk}E_k,\ D_i = e_{ijk}\varepsilon_{jk} + \alpha_{ij}E_j,$$

where C, ε, e, E and α denote the elastic tensor, the linearized strain tensor, the piezoelectric tensor, the electric field and the dielectric tensor, respectively. The electric current and linearized strain tensors are related to the electric potential φ and to the displacement vector u through:

$$E_i = -\frac{\partial \phi}{\partial x_i},\quad \varepsilon_{ij} = \frac{1}{2}\left(\frac{\partial u_i}{\partial x_j} + \frac{\partial u_j}{\partial x_i}\right).$$

The above equations are completed by appropriate boundary conditions on corresponding portions of the boundary of the domain Ω describing the system. Then, a classical finite element procedure is employed to solve the above problem.

3. Results and Discussion

3.1. Piezoelectric effect characterization

The fabrication process of highly populated cluster-free ZnO nanowire arrays is displayed in Figure 1a. First, the morphology of the as-grown (PMMA-free) ZnO nanowire arrays has been characterized using the SEM (Figure 1b). The cross-sectional SEM images clearly display some

Journal of Materials Chemistry C Accepted Manuscript

clusters of nanowires (red arrows in Figure 1b). The presence of clusters in the NW array produces an effective reduction of the currents generated, as confirmed by CAFM current maps (see Figure S1 in the supporting information). Therefore, reducing the presence of NW clusters should be a priority. Figures 1c and 1d show the cross-sectional SEM images of the sample after the spin coating and oxygen plasma etching steps (respectively) using optimized parameters: spin coating at 4000 rpm during 3 minutes and etching for 1.5 minutes. As it can be observed, the optimized nanogenerator shows effective NW-to-NW separation, leading to a vertical and parallel array. During spin coating, the PMMA flows in between the nanowires forming a homogeneous NWs/PMMA mesh, as corroborated by EDX (Figures S2 and S3). Our observations indicate that a faster spin coating speed contributes to spread the PMMA gel, leading to a better interface free of voids or bubbles (see Figure S4). Once the sample is fully covered by PMMA, nanowires movement is restricted (Figure 1c), which avoids current generation (and transmission, as the PMMA is an insulator). In the second step, the nanowires are partially liberated by etching the top part of the PMMA film by oxygen plasma treatment, allowing their movement and piezo-potential generation (Figure 1d). In order to guarantee that the oxygen plasma treatment doesn't affect the morphology and the piezoelectric properties of ZnO nanowires, SEM and CAFM measurements were conducted in PMMA-free samples before and after an aggressive oxygen plasma treatment of 5 minutes (which is three times longer than that used in optimized samples). The data (shown in Figure S5) indicate that the NWs hold very similar morphology and current generation capability than the fresh sample, discarding the damage of the nanowires during the oxygen plasma step. Further structural characterization by TEM revealed similar sharp profile and crystalline ZnO structure, and no signs of clear structural damage were observed (Figure S6). Our experiments and calculations demonstrate that the

Journal of Materials Chemistry C Accepted Manuscript

thickness of the PMMA film can be optimized to produce maximum currents. The optimized etching time should achieve a PMMA film enough thick to get away NWs collision, and at the same time it should be as thin as possible to allow NWs movement. In the following we present how such compromise can be achieved.

Figure 2 shows the surface roughness measured with AFM for: (a) the as-fabricated (PMMA-free) NWs array, (b) the same sample after PMMA spin coating, and (c-h) the NWs/PMMA mesh after different etching times (0.5, 1, 1.5, 2, 3 and 4 minutes). For the PMMA-free sample, a high density of tilted nanowires that collide and form clusters can be observed, and the top circular contour of the nanowires cannot be clearly distinguished (inset in Figure 2a and Figure S7). After the spin coating step, the nanowires are completely wrapped by PMMA, leading to a very good vertical alignment and showing very clear circular shapes (Figure 2b). During the etching process, the PMMA layer is being progressively removed, and after long times the NWs array recovers its initial configuration (Figures 2a and 2h are very similar). During this process, we observe one time for which the profile of the NWs/PMMA mesh shows an optimized topographic profile free of NWs clusters (1.5 minutes, Figure 2e). This behavior can be more clearly observed in the cross-sectional profiles of the topographic AFM (Figures 2i, 2j and 2k). The optimized sample shows the largest surface roughness, produced by the separation of the NWs, which allows AFM tip penetration between them.

As the goal of this methodology is to enhance the piezoelectric signal, we conduct exhaustive nanoscale electrical analysis by means of CAFM, and the surface of all the samples is scanned using metal-varnished AFM tips. In order to quantify only the piezotronic effect, we avoided the

Journal of Materials Chemistry C Accepted Manuscript

influence of light by turning off the AFM light bank during the measurements. Figure 3 shows the current maps with a superimposed cross section. The same Z-scale (-20 pA to 20 pA) is used for all samples to facilitate comprehensive comparison. The cross sections were taken in diagonal from the left-bottom to top-right corners of each image. The PMMA-free sample (Figure 3a) shows peak currents up to 5 pA spread along the boundaries of the nanowires, in agreement with those previously reported in the literature [27-28, 31]. Nevertheless, it should be highlighted that the current values here reported are obtained using tips with an specific spring constant, tip radius an metallic alloy, and therefore unless other AFM-based works in the literature use strictly the same types of tips, direct comparisons are not allowed (further discussion of this behavior is presented in the supporting information, Figure S8). By comparing all samples in Figure 3 it can be observed that the as-grown sample shows larger current spots that drive low currents (probably related to the formation of NWs clusters), as already displayed in Figure S1. As expected, after the coating step no current spots are displayed in the current map (Figure 3b), due to the presence of insulating PMMA. After partial removal of PMMA, the current initially increases with the etching time (Figures 3c, 3d and 3e), until reaching a maximum after 1.5 minutes etching. Interestingly, after short time etching (below 1.5 minutes) not only the currents driven by the nanowires increase, but also the size of the conductive spots decrease (see Figure S9), indicating the effective suppression of NWs clusters, in agreement with the topographic maps. The suppression of NWs clusters is important as they require larger forces to be moved, leading to a remarkable reduction of the device performance. As a result, the amount of energy generated is greatly enhanced. For longer etching times, the nanowires start to bundle again, reducing the currents generated. On one hand, the larger aspect ratio of the freestanding (non PMMA buried) part of the NWs at longer etching times produces larger

Journal of Materials Chemistry C Accepted Manuscript

currents but, on the other, longer aspect ratios also facilitate the NW clustering. Therefore, the optimized sample shows the best compromise between both effects, leading to a maximized current.

The reliability of the devices here presented has been analyzed by measuring sequences of currents maps, which show that the morphology and performance is maintained despite the NWs movement (see Figure S10). Here probably the PMMA is providing additional mechanical reinforcement [30]. Moreover, we scanned the optimized sample after storing it 3 months, and the performance was again similar (see Figure S10), indicating the good stability of the device and the high reliability of the data here presented. In order to allow an effective comparison, we quantified the total amount of current collected in the current maps, using the software of the AFM and applying a threshold right above the electrical noise level. This analysis (Figure S9) reveals that the currents generated per area unit in the PMMA-free sample are 5.37 $pA/\mu m^2$, while that number raises up to 426.12 $pA/\mu m^2$ for the optimized device, leading to a net performance increase of a factor ~80. These numbers are similar to those reported by other groups [14], but again we would like to emphasize that comparing quantified CAFM data from paper-to-paper is not meaningful, given the large variability to which this technique is exposed (as above mentioned).

We corroborate the performance enhancement in the optimized device analyzing the currents generated by all cells. The current maps are analyzed using the software of the CAFM, and the currents driven by the spots are statistically displayed in Figure 4. The data clearly display that, for the optimized sample, the amount of conductive spots detected and their currents is larger.

Journal of Materials Chemistry C Accepted Manuscript

Figure 4 also clearly displays the two well-differenced regions: I) an initial increase for short etching times below 1.5 nm due to the reduction of PMMA height, and II) a decrease of the cell performance at longer times due to complete removal of the PMMA, leading again to NWs clustering.

3.2. Finite element method calculations

In order to study the piezoelectric effects associated with bending of the nanowires in the device, the piezo potential along a single nanowire was simulated by FEM calculations. It consists of ZnO whose main growth direction is [0001] and having a hexagonal cross section. The length L of the nanowire is 600 nm, the diameter d is 50 nm. A force F = 80 nN was applied to a surface of 50 nm × 5 nm on one side of the nanowire. Figure 5a shows the schematic of such configuration. The material was modeled as having a piezoelectric behavior of coefficients whose values are given in Table 1. The problem is solved by the finite element method. It is assumed that there is no electric field applied and no body forces. The lateral displacement of the nanowire (in the direction of X-axis), is 97.79 nm and the electric potential at a height of 600 nm is ±0.45 V. Figure 5b shows the result of calculating the electric potential for bending the nanowire with a numerical code bar besides. In the following, we study the sensitivity to the maximum potential obtained for a constant applied force of 80 nN on the surface of 50 nm × 5 nm and different ratios of aspects L/d. The length L = 600 nm is fixed and the diameter varies between d = 5 nm and d = 50 nm. In Figure 5c, we compare the results obtained using the calculations with the ones in the literature[32]. The high consistency achieved validates our numerical code developed in this work. These calculations allow us to observe that the maximum

Journal of Materials Chemistry C Accepted Manuscript

electric potential is obtained for the ratio L/d maximum when taking clustering effect into consideration.

We then investigate the influence of varying the height of PMMA. We conduct a simulation involving a single nanowire in a volume of PMMA. A force of 1 nN is applied laterally on the nanowire. The height varies between 250 nm PMMA and 2.75 μm. In Figure 6 the potential vs. PMMA height is plotted and, as it can be clearly seen, a reduction of the PMMA height increases the piezoelectric potentials generated. This calculation clearly supports the upward current trend observed in Figure 4 (region I). In that case, larger etching times represent lower PMMA heights. The main explanation for this phenomenon is that the part of the NWs encapsulated by the PMMA cannot flex, leading to a shorter effective height of the NWs and a smaller L/d ratio.

3.3. Photoresponse enhancement in hybrid nanogenerators

Apart from clear enhancement of piezotronic effect, we observe a side effect that may be useful for hybrid energy converters. Vertically aligned ZnO nanowire arrays have been also used for the scavenging of solar energy. For example, Wu et al. [33] used atmospheric pressure plasma treatment to fabricate ZnO-deposited photodetectors with high sensitivity. In this section, we also analyze the effect of cell optimization on the photoresponse of the nanowries array. To do so, we combine the light bank of the CAFM adjusted at different intensities. Sarah et al. [34] used this setup to monitor local current generation in solar cells based on arrays of GaN/InGaN nanowires.

We collected series of current maps for the as-fabricated (PMMA-free) and optimized samples using different light intensities (Figure 7). The first observation is that, for the PMMA-free

Journal of Materials Chemistry C Accepted Manuscript

sample, the currents measured for a light intensity of 0% are similar to those reported in Figure 3a (5 pA, which was collected in the dark), and the current increases with the light intensity up to 15 pA. This current enhancement is related to the generation of electron-hole pairs due to the photoelectric effect, as previously demonstrated [33]. This experiment was repeated for the samples etched during 0.5, 1.5 and 3 min, and the one etched for 1.5 min is again the one that shows the largest currents. This large current enhancement should be related to the effective separation of the nanowires (see Figures 1 and 2), which increases the surface area available for the photoelectric effect. Also noteworthy, the part of the NW that is encapsulated with PMMA may also be generating photocurrents, as this polymer is transparent.

4. Conclusions

In conclusion, we have developed a simple methodology to enhance the performance of ZnO nanowires based hybrid energy harvesters by avoiding NWs clustering. To do so, we intercalate a spin-coated flexible polymer layer between the nanowires, and the performance of the cell is optimized by tuning the height of the polymer using an oxygen plasma etching step. In the resulting optimized cell, the piezoelectric signal is enhanced in a factor 80, compared to the standard counterpart, and the photoelectric effect also shows notable improvement. The experimental observations have been corroborated by finite element method calculations, which demonstrate the link between the PMMA height and the generated piezo potential along the nanowires.

Journal of Materials Chemistry C Accepted Manuscript

FIGURES

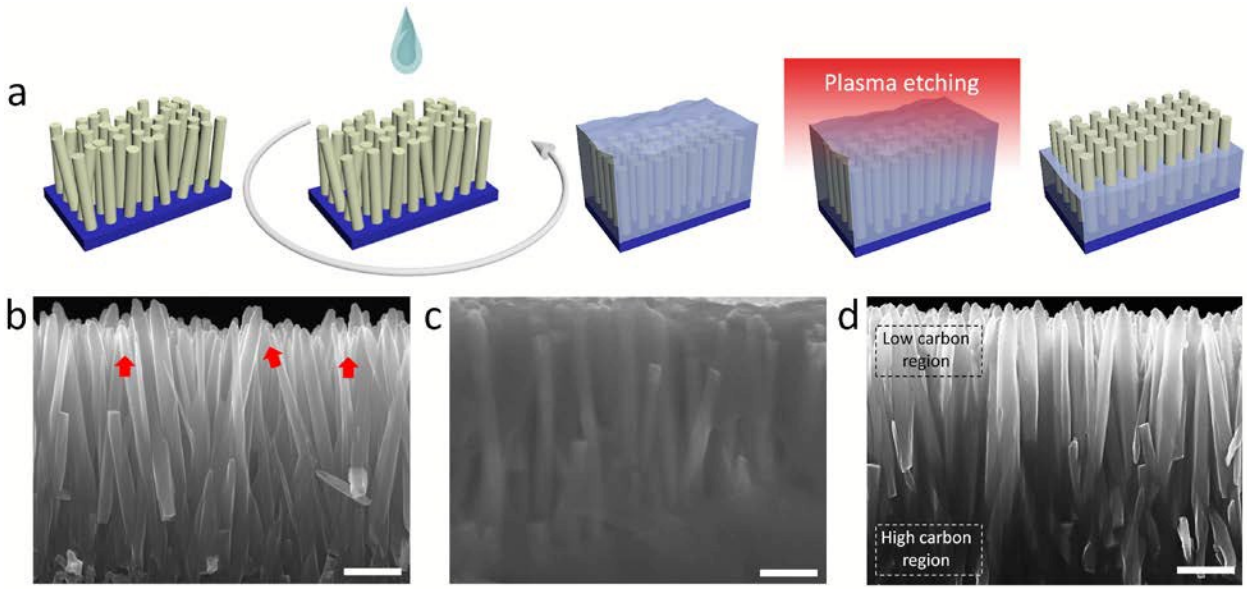

Figure 1. (a) Fabrication process of vertically aligned ZnO nanowire arrays. SEM cross-view of (b) PMMA-free ZnO nanowire arrays, (c) ZnO nanowire arrays totally wrapped by PMMA, and (d) homogeneous NWs/PMMA mesh after optimized etching time. The dark areas in the bottom part of (d) correspond to PMMA, which has been corroborated by larger amounts of carbon in the EDX (see Figure S2 and S3 in the supporting information). The scale bars in b-d are 1 μm.

Journal of Materials Chemistry C Accepted Manuscript

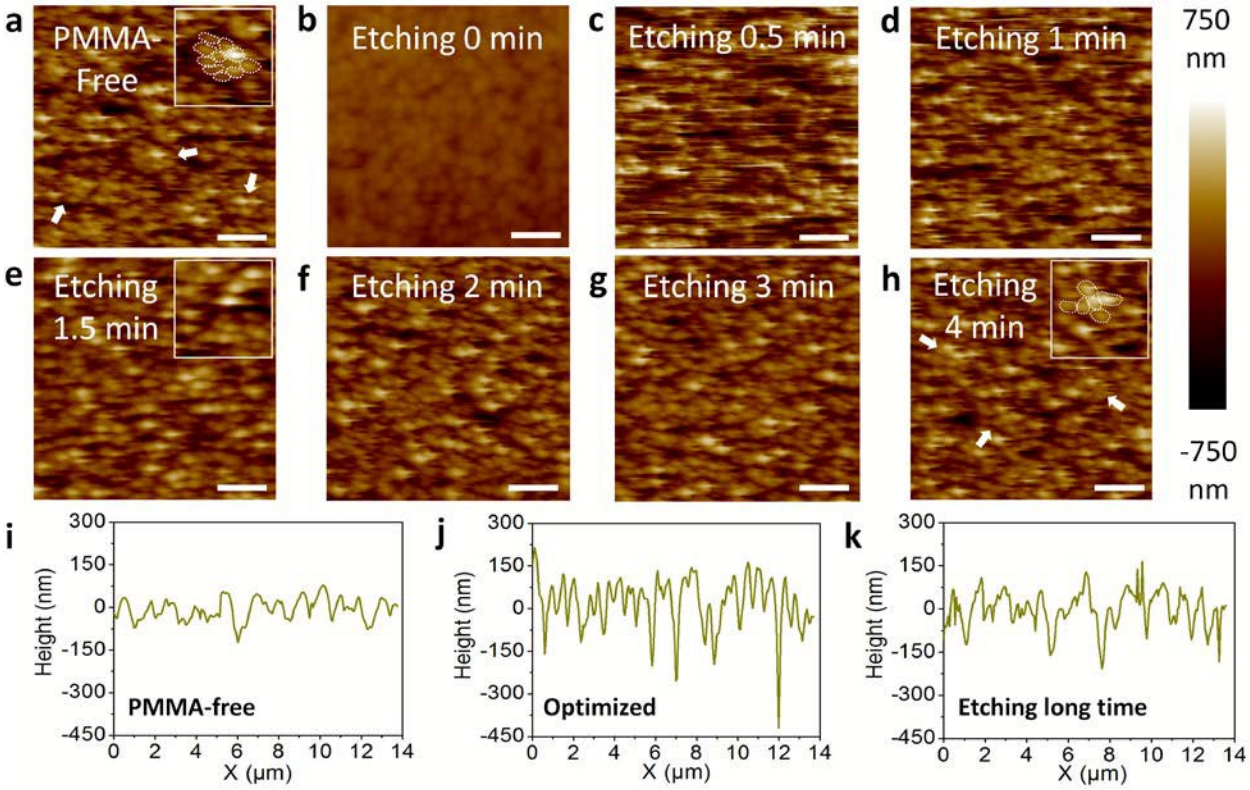

Figure 2. (a) AFM topography image of PMMA-free NWs, (b) AFM topography image of grown NWs totally wrapped with PMMA, and (c)-(h) AFM topography images of NWs penetrated with PMMA etched for 0.5, 1, 1.5, 2, 3 and 4 minutes respectively. (i), (j) and (k) show the cross-sectional profiles of topographic AFM images after each step. The scale bars in a-h are 2 μm.

Journal of Materials Chemistry C Accepted Manuscript

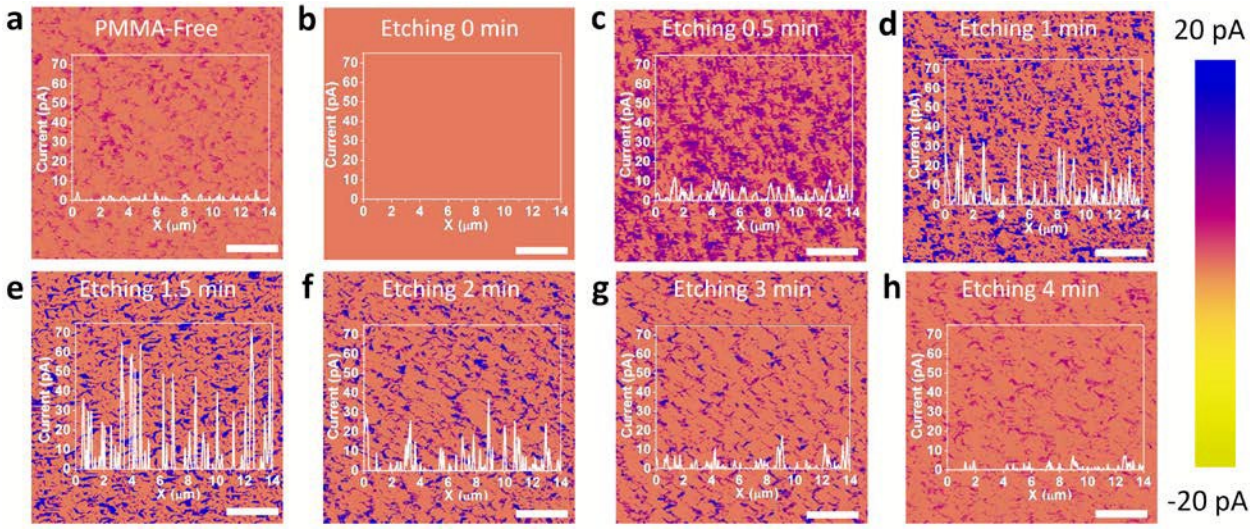

Figure 3. (a) current and cross-sectional maps of PMMA-free NWs, (b) current and cross-sectional maps of grown NWs totally wrapped with PMMA, and (c)-(h) current and cross-sectional maps of NWs penetrated with PMMA etched for 0.5, 1, 1.5, 2, 3 and 4 minutes respectively. The scale bars in a-h are 2 μm.

Journal of Materials Chemistry C Accepted Manuscript

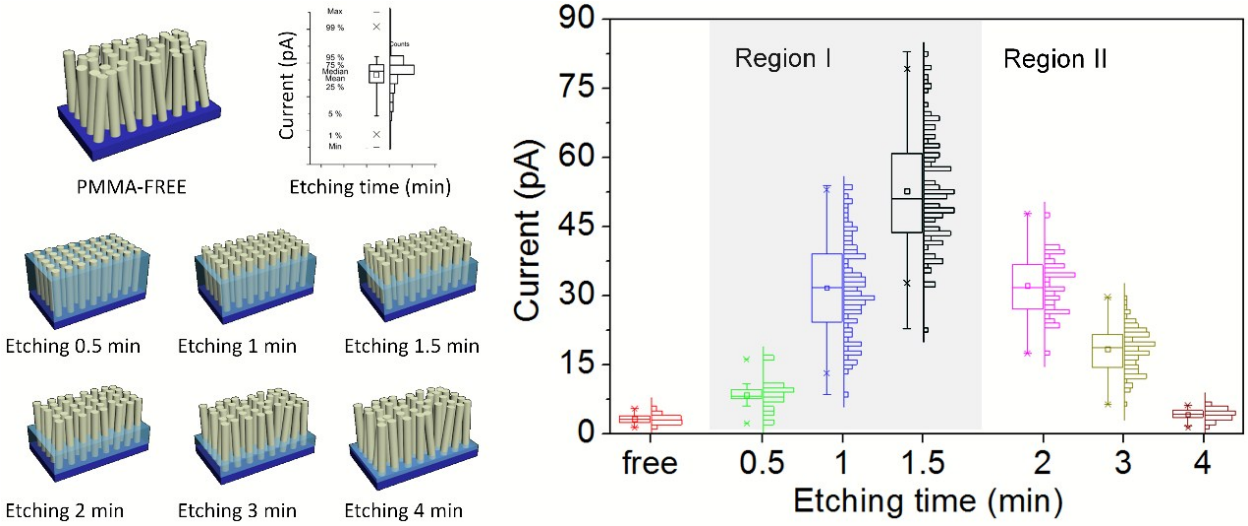

Figure 4. A box chart of the measured current data. Including the sample of PMMA-free NWs and 6 other samples etched for 0.5min, 1 min, 1.5 min, 2 min, 3 min and 4 min respectively.

Journal of Materials Chemistry C Accepted Manuscript

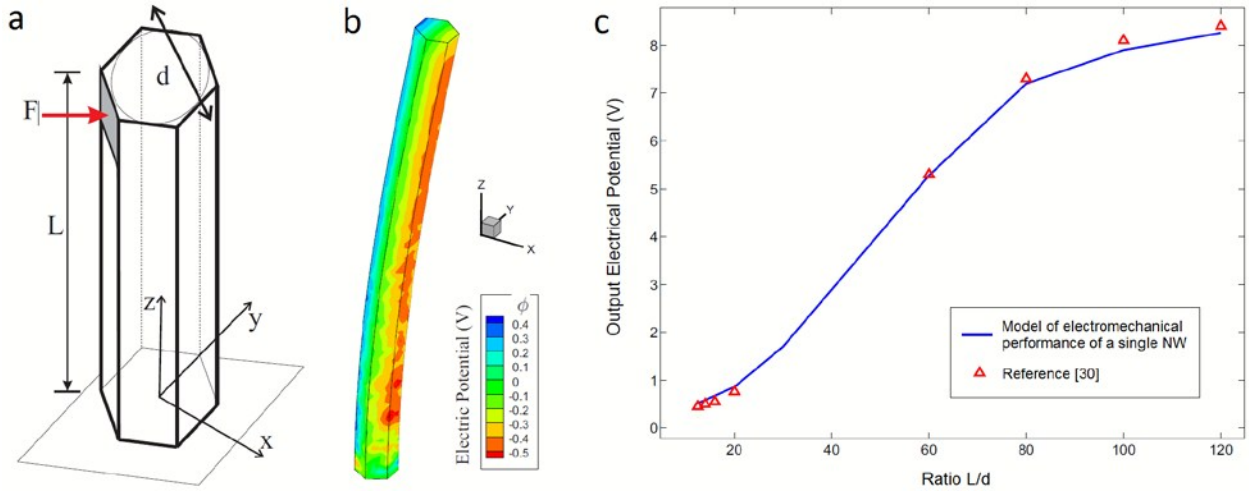

Figure 5. Validation of the finite element method model. (a) geometry of the nanowire simulated (d = 50 nm and L = 600 nm). A force of 80nN has been applied to the top of the nanowire (in a surface area of 250 nm^2). We selected these parameters to validate our model with those reported in reference [30]. (b) electric potential in the nanowire depicted in (a). (c) maximum electric potential versus aspect ratio calculated.

Journal of Materials Chemistry C Accepted Manuscript

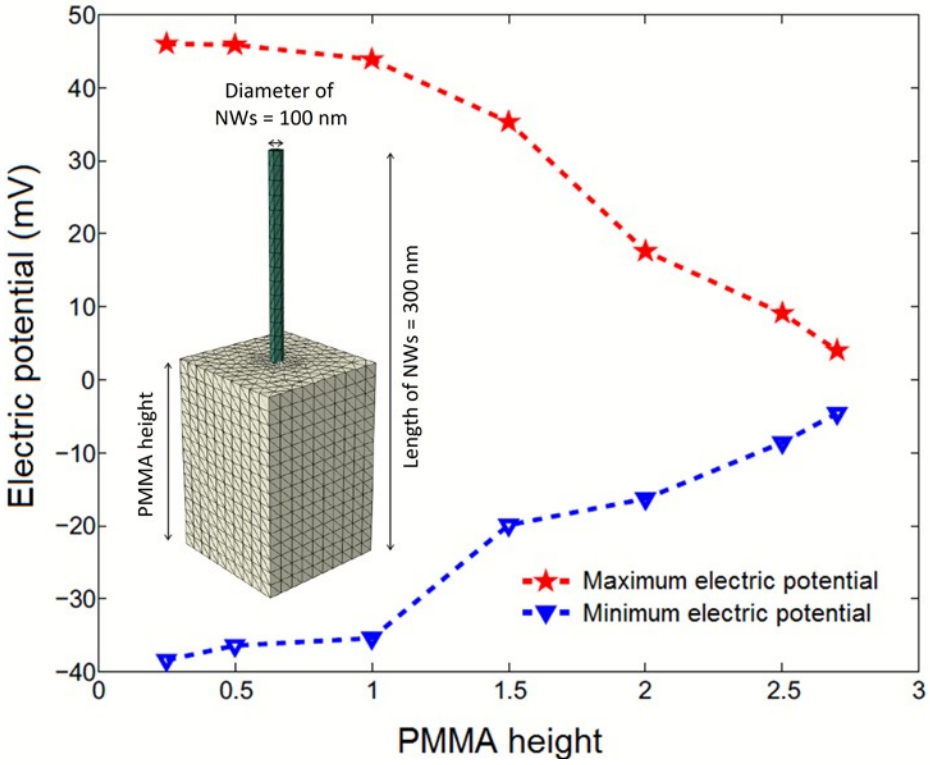

Figure 6. Finite elements method calculation of the deformation and electric potential for a single nanowire embedded in polymer matrix of height (a) H = 2.5 μm, (b) H = 2 μm, and (c) H = 1.5 μm, for a prescribed lateral force F = 1 nN; (d) electric potential versus PMMA height. The inset displays the configuration used for this simulation.

Journal of Materials Chemistry C Accepted Manuscript

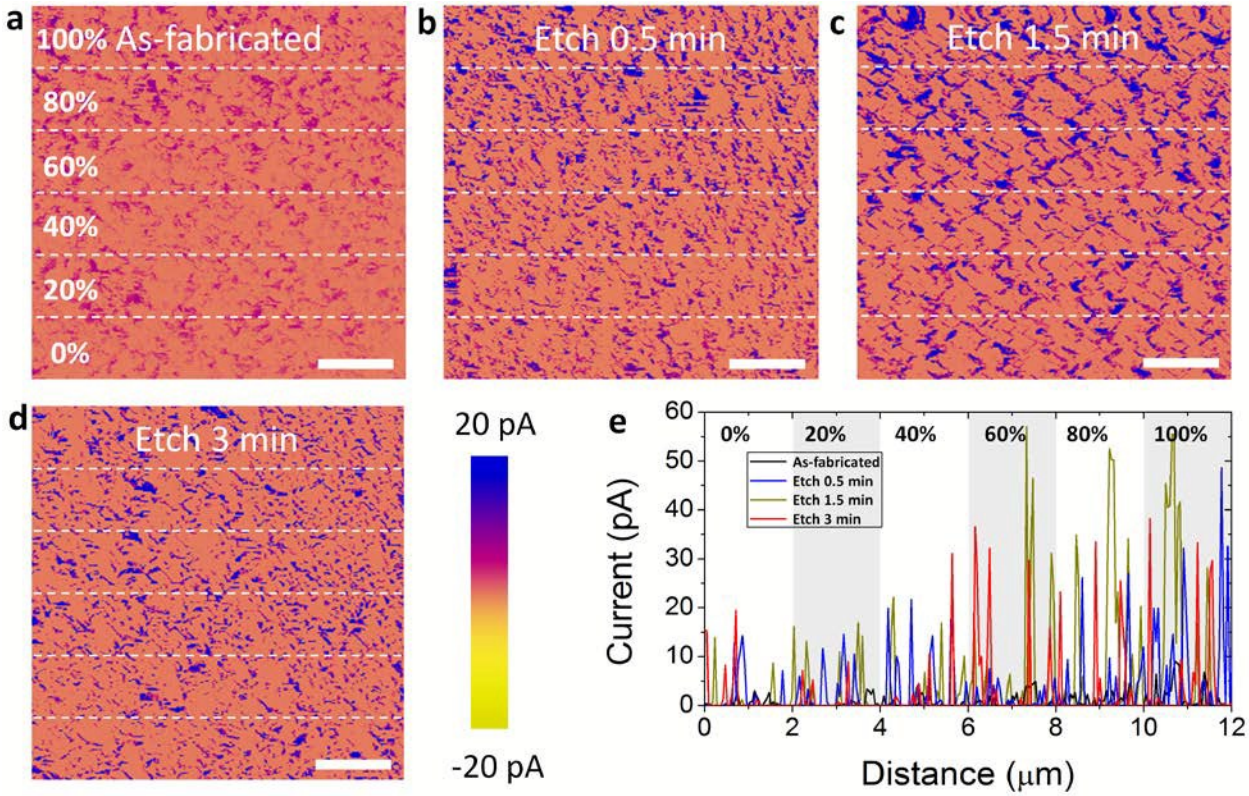

Figure 7. (a-d) CAFM current maps mixed with photoelectric and piezoelectric current under different light intensity illumination generated by as-fabricated sample and the PMMA-NW samples etched for 0.5 min, 1.5 min (optimized), 3 min respectively, (e) cross-sectional current maps mixed with photoelectric and piezoelectric current under different light intensity illumination generated by as-fabricated sample and the PMMA-NW samples etched for 0.5 min, 1.5 min (optimized), 3 min respectively. The scale bar in a-d is 2 μm.

Journal of Materials Chemistry C Accepted Manuscript

TABLES

Table 1. Properties of ZnO NWs in the device

Elastic coefficients (GPa)	C_{11}	C_{33}	C_{13}	C_{12}	C_{55}
	203.3	215.1	103.3	117.8	34.0
Piezoelectric coefficients (C/m^2)	e_{31}		e_{33}	e_{15}	
	-0.561		1.276	-0.535	
Relative permittivity of the dielectric coefficients	α_{11}		α_{22}	α_{33}	
	7.77		7.77	8.91	

ASSOCIATED CONTENT

Supporting Information. Additional information about fabricated samples and sample performance characterization is provided in the supporting information. This material is available free of charge via the Internet at http://pubs.rsc.org.

AUTHOR INFORMATION

Corresponding Author

* Mario Lanza, Institute of Functional Nano and Soft Materials (FUNSOM), Soochow University, Suzhou 215123, China

Journal of Materials Chemistry C Accepted Manuscript

Author Contributions

M. L. and J. Y. designed the research plan. J. H. and C. P. synthesized the samples, characterized the samples and wrote the manuscript. M. H., A. M. and G. C. carried out the simulation. M. L., H. D. and E. G.-G. supervised the manuscript. All the authors discussed the results and approval the manuscript.

Funding Sources

This work has been partially supported by the Young 973 National Program of the Chinese Ministry of Science and Technology (grant no. 2015CB932700), the National Natural Science Foundation of China (grants no. 61502326, 41550110223), the Jiangsu Government (grant no. BK20150343) and the Ministry of Finance of China (grant no. SX21400213). M. Lanza acknowledges generous funding from the Young 1000 Talent Program of China. The Collaborative Innovation Center of Suzhou Nano Science & Technology, the Jiangsu Key Laboratory for Carbon-Based Functional Materials & Devices and the Priority Academic Program Development of Jiangsu Higher Education Institutions are also acknowledged.

ACKNOWLEDGMENT

This work has been partially supported by the Young 973 National Program of the Chinese Ministry of Science and Technology (grant no. 2015CB932700), the National Natural Science Foundation of China (grants no. 61502326, 41550110223), the Jiangsu Government (grant no. BK20150343) and the Ministry of Finance of China (grant no. SX21400213). M. Lanza acknowledges generous funding from the Young 1000 Talent Program of China. The

Journal of Materials Chemistry C Accepted Manuscript

Collaborative Innovation Center of Suzhou Nano Science & Technology, the Jiangsu Key Laboratory for Carbon-Based Functional Materials & Devices and the Priority Academic Program Development of Jiangsu Higher Education Institutions are also acknowledged.

ABBREVIATIONS

NW: nanowire; SEM: scanning electron microscopy; AFM: atomic force microscopy; CAFM: conductive atomic force microscopy; FEM: finite element method.

REFERENCES

[1] Pradel, K. C.; Wu, W. Z.; Ding, Y.; Wang, Z. L. Solution-Derived ZnOHomojunction Nanowire Films on Wearable Substrates for Energy Conversion and Self-Powered Gesture Recognition. *Nano Lett.* 2014, *14*, 6897- 6905.

[2] Nabar, B. P.; Butler, Z. C.; Butler, D. P. Piezoelectric ZnONanorod Carpet as a NEMS Vibrational Energy Harvester. *Nano Energy***2014**, *10*, 71-82.

[3] Nour, E. S.; Sandberg, M. O.; Willander, M.; Nur, O. Handwriting Enabled Harvested Piezoelectric Power Using ZnO Nanowires/Polymer Composite on Paper Substrate. *Nano Energy* **2014**, *9*, 221-228.

[4] Udom, I.; Ram, M.; Stefanakos, E.; Hepp, A. F.; Goswami, D. Y. One Dimensional-ZnO Nanostructures: Synthesis, Properties and Environmental Applications Mater. *Sci. Semicond. Process.* **2013**, *16*, 2070-2083.

[5] Wang, Z. L. Triboelectric Nanogenerators as New Energy Technology for Self-Powered Systems and as Active Mechanical and Chemical Sensors. *ACS NANO* **2013**, *7*, 9533-9557.

Journal of Materials Chemistry C Accepted Manuscript

[6] Chang, Y. C. Temperature-dependence Cathodoluminescence of Ultra-Sharp ZnONanopagoda Arrays. *J. Alloys Compd.* **2014**, *617*, 16-20.

[7] Jorge, R. M.; Elena, N. A.; Rocio, R.; Francisco, M.; Ricardo, S.; Ramos, B. J. R.; Enrique, A. D. Electrochemically Grown Vertically Aligned ZnONanorod Array/p+-Si (100) Heterojunction Contact Diodes.*Thin Solid Films* **2013**, *548*, 235-240.

[8] Xu, C.; Wang, X. D.; Wang, Z. L. Nanowire Structured Hybrid Cell for Concurrently Scavenging Solar and Mechanical Energies.*J. Am. Chem. Soc.* **2009**, *131*,5866-5872.

[9] Kathalingam, A.; Valanarasu, S.; Senthilkumar, V.; Rhee, J. K. Piezo and Photoelectric Coupled Nanogenerator Using CdSe Quantum Dots Incorporated ZnO Nanowires in ITO/ZnO NW/Si Structure. *Mater. Chem. Phys.* **2013**, *138*, 262-269.

[10] Yang, Y.; Zhang, H. L.; Zhu, G.; Lee, S. M.; Lin, Z. H.; Wang, Z. L. Flexible Hybrid Energy Cell for Simultaneously Harvesting Thermal, Mechanical, and Solar Energies. *ACS Nano* **2013**, *7*, 785-790.

[11] Wen, Z.; Zhu, L. P.; Zhang, Z. Y.; Ye, Z. Z. Fabrication of Gas Sensor Based On Mesoporous Rhombus-Shaped ZnO rod Arrays. *Sens. Actuators, B* **2015**, *208*, 112-121.

[12] Lim, Z. H.; Chia, Z. X.; Kevin, M.; Wong, A. S. W.; Ho, G. W. A Facile Approach TowardsZnONanorods Conductive Textile for Room Temperature Multifunctional Sensors. *Sens. Actuators, B* **2010**, *151*, 121-126.

[13] San, X. G.; Wang, G. S.; Liang, B.; Song, Y. M.; Gao, S. Y.; Zhang J. S.; Meng F. L. Catalyst-free Growth of One-Dimensional ZnO Nanostructures on SiO_2 Substrate and in Situ Investigation of Their H_2 Sensing Properties. *J. Alloys Compd.* **2015**, *622*, 73-78.

[14] Wang, Z. L.; Song, J. H. Piezoelectric Nanogenerators Based on Zinc Oxide Nanowire Arrays. *Science* **2006**, *312*, 242-246.

Journal of Materials Chemistry C Accepted Manuscript

[15] Zhong, M.; Sato, Y. K.; Kurniawan, M.; Apostoluk, A.; Masenelli, B.; Maeda, E.; Lkuhara, Y.; Delaunay, J. ZnO Dense Nanowire Array on a Film Structure in a Single Crystal Domain Texture for Optical and Photoelectrochemical Applications. *Nanotechnology* **2012**, *23*, 495602.

[16] Lin, C. J.; Chen, S. Y.; Liou, Y. H. Wire-Shaped Electrode of CdSe-sensitized ZnO Nanowire Arrays for Photoelectrochemical Hydrogen Generation. *Electrochem. Commun.* **2010**, *12*, 1513-1516.

[17] Kang, Z.; Gu, Y. S.; Yan, X. Q.; Bai, Z. M.; Liu, Y. C.; Liu, S.; Zhang, X. H.; Zhang, Z.; Zhang, X. J.; Zhang, Y. Enhanced Photoelectrochemical Property of ZnoNanorods Array Synthesized on Reduced Graphene Oxide for Self-Powered Biosensing Application. *Biosens. Bioelectron.* **2015**, *64*, 499-504.

[18] Dhara, S.; Giri, P. K. On the Origin of Enhanced Photoconduction and Photoluminescence from Au and Ti Nanoparticles Decorated Aligned ZnO Nanowire Heterostructures.*J. Appl. Phys.* **2011**, *110*, 124317.

[19] Xu, S.; Lao, C. S.; Weintraub, B.; Wang, Z. L. Density-Controlled Growth of Aligned ZnO Nanowire Arrays by Seedless Chemical Approach on Smooth Surfaces.*J. Mater. Res.***2008**, *23*, 2072-2077.

[20] Ge, X.; Hong, K.; Zhang, J.; Liu, L. Q.; Xu, M. X. A. Controllable Microwave-Assisted Hydrothermal Method to Synthesize ZnO Nanowire Arrays as Recyclable Photocatalyst. *Mater. Lett.* **2015**, *139*, 119-121.

[21] Nam, G.; Park, Y.; Ji, L.; Kim, B.; Lee, S. H.; Kim, D. Y.; Kim, S.; Kim, S. O.; Leem, J. Y. Facile Synthesis and Enhanced Ultraviolet Emission of ZnONanorods Prepared by Vapor-Confined Face-to-Face Annealing. *ACS Appl. Mater. Interfaces* **2015**, *7*, 873-879.

Journal of Materials Chemistry C Accepted Manuscript

[22] Kar, J. P.; Kim, S.; Shin, B.; Park, K.I.; Ahn, K. J.; Lee, W.; Cho, J. H.; Myoung, J. M. Influence of Sputtering Pressure on Morphological, Mechanical and Electrical Properties of Al-Doped Zno Films. *Solid-State Electronics* **2010**, *54*, 1447–1450.

[23] Yang, M.; Kim, H. C.; Hong, S. H. Growth of ZnONanorods on Fluorine-Doped Tin Oxide Substrate Without Catalyst By Radio-Frequency Magnetron Sputtering. *Thin Solid Films* **2014**, *573*, 79-83.

[24] Nicaise, S. M.; Cheng, J. J.; Kiani, A.; Gradečak, S.; Berggren, K. K. Control of Zinc Oxide Nanowire Array Properties with Electron-Beam Lithography Templating for Photovoltaic Applications. *Nanotechnology* **2015**, *26*, 075303.

[25] Khranovskyy, V.; Yakimova, R. Morphology Engineering of Zno Nanostructures. *Physica B* **2012**, *407*, 1533-1537.

[26] Xu, S.; Wei, Y. G.; Liu, J.; Yang, R. S.; Wang, Z. L. Integrated Multilayer Nanogenerator Fabricated Using Paired Nanotip-to-Nanowire Brushes.*Nano Lett.* **2008**, *8*, 4027-4032.

[27] Hsu, C. L.; Chen, K. C. Improving Piezoelectric Nanogenerator Comprises ZnO Nanowires by Bending the Flexible PET Substrate at Low Vibration Frequency. *J. Phys. Chem.* **2012**, *116*,9351-9355.

[28] Lanza, M.; Reguant, M.; Zou, G.; Lv, P.; Li, H.; Chin, R.; Liang, H.; Yu, D.; Zhang, Y.;Liu, Z.; Duan H. High Performance Piezoelectric Nanogenerators Using Two-Dimensional Flexible Top Electrodes.*Adv. Mater. Interfaces* **2014**, *1*, 1300101.

[29] Kumar, B.; Lee, K. Y.; Park, H. K.; Chae, S. J.; Lee, Y. H.; Kim, S. W. Controlled Growth of Semiconducting Nanowire, Nanowall, and Hybrid Nanostructures on Graphene for Piezoelectric Nanogenerators. *ACS Nano* **2011**, *5*,4197-4204.

Journal of Materials Chemistry C Accepted Manuscript

[30] Gao, P. X.; Song, J. H.; Liu, J.; Wang, Z. L. Nanowire Piezoelectric Nanogenerators on Plastic Substrates as Flexible Power Sources for Nanodevices. *Adv. Mater.* **2007**, *19*, 67-72.

[31] Li, Z.; Zhu, G.; Yang, R. S.; Wang, A. C.; Wang, Z. L. Muscle-Driven in Vivo *Nanogenerator*. *Adv. Mater.* **2010**, *22*, 2534-2537.

[32] Gao, Y. F.; Wang, Z. L. Electrostatic Potential in a Bent Piezoelectric Nanowire. The Fundamental Theory of Nanogenerator and Nanopiezotronics.*Nano Lett.* **2007**, *7*, 2499-2505.

[33] Wu, T. H.; Cheng, I. C.; Hsu, C. C.; Chen, J. Z. UV Photocurrent Responses of ZnO and MgZnO/ZnO Processed by Atmospheric Pressure Plasma Jets. *J. Alloys Compd.* **2015**, *628*, 68-74.

[34] Howell, S. L.; Padalkar, S.; Yoon, K. H.; Li, Q. M.; Koleske, D. D.; Wierer, J. J.; Wang, G. T.; Lauhon, L. J. Spatial Mapping of Efficiency of GaN/InGaN Nanowire Array Solar Cells Using Scanning Photocurrent Microscopy. *Nano Lett.* **2013**, *13*, 5123-5128.

Journal of Materials Chemistry C Accepted Manuscript